



CrossMark
 click for updates

Cite this: *RSC Adv.*, 2015, 5, 88719

Superhigh-speed unidirectional rotation of a carbon nanotube in a sheared fluid and its decoupled dynamics†

Ruo-Yu Dong and Bing-Yang Cao*

The superhigh-speed unidirectional rotation of a carbon nanotube (CNT) induced by a linear shear flow is investigated by molecular dynamics simulations. We have identified three rotational types: "continuous rotation", "interrupted rotation" and "simple oscillation", corresponding to a decreased number of unidirectional rotation circles over the same time duration. It was found that the unidirectional motion and oscillation respectively originate from the applied shear and rotary Brownian motion by a decoupled analysis of the rotational features. The angular velocity of the unidirectional motion is over one order of magnitude larger than the Jeffery's theory. To construct a CNT-based rotary motor with good performance, the high-speed unidirectional angular velocity can be achieved by carefully selecting the shear rate (e.g. $\sim 2 \times 10^8$ rad s^{-1} at 35 GHz) and the continuous rotating state can be approached by using a low aspect ratio carbon nanotube.

Received 15th September 2015

Accepted 14th October 2015

DOI: 10.1039/c5ra18901b

www.rsc.org/advances

1. Introduction

Nanomachine engineering has attracted intense research interest, among which is the desire to construct delicate rotary nanomotors. In biological systems, the typical study subjects of molecular motors include F_0F_1 -ATPase¹ and flagella,² which can convert chemical energy to mechanical movements and serve as functional parts in many natural-synthetic hybrid systems.^{3,4} These natural or semi-natural motors suffer from restrictions of the environmental conditions,⁵ and the demands of wholly artificial nano-systems⁶⁻⁹ have accordingly arisen. Thus, researchers have witnessed a variety of studies utilizing magnetic field,¹⁰ electric field^{11,12} or polarized light¹³ to realize unidirectional rotation of nanoparticles, and the applications are extended from biological issues to micro/nanofluidics and micro/nanoelectromechanical systems (MEMS/NEMS). Carbon nanotube (CNT) based motors are the current focus, due to CNT's great mechanical and electronic properties as well as its biocompatibility¹⁴ and near-infrared fluorescent features,¹⁵ all of which make CNTs a suitable component for the above listed areas. For instance, one of these topics is the double-walled CNT rotating systems composed of a stator and a rotor without liquid media.^{16,17}

When CNTs are dispersed in suspensions, an easy way to control its rotational motion is by imposing a fluid flow. Studies on this issue were mostly focusing on the orientation state^{18,19} and related rheological phenomena²⁰ of CNT suspensions. However, the related motor study is scarce, only recently a nanoturbine model consisted of a CNT and three graphene blades was designed to rotate unidirectionally in water flow by molecular dynamics (MD) simulations.²¹ Some light was shed on this problem by Jeffrey²² in 1922 who theoretically predicted that a single ellipsoid would rotate unidirectionally in a single parameter family of closed orbits in a sheared viscous fluid. Later studies extended the Jeffery orbits to rod-shaped particles,²³ just like CNT, and considered the influences of rotary Brownian motion.^{24,25} The MD results²⁵ confirmed that the rotation period of a low aspect ratio CNT in linear shear agrees with Jeffery's theory with only a slight difference. The flow-induced nanoparticle rotation is actually a coupled effect from the applied shear and Brownian rotation, whose impacts have not been distinguished from each other previously. This study thus provides detailed analyses on a single CNT's two-dimensional (2D) rotational behavior and dynamics as well as the decoupled features and their origin by MD simulations. The simulated very small aspect ratio CNT is treated as a rigid rod^{19,25} without considering the effect of deformation.^{26,27} The high-speed unidirectional rotation is observed and the criteria to achieve it are discussed to better facilitate the CNT-based rotary motor design.

2. Simulation methods

Fig. 1(a) exhibits a capped CNT embedded in fluid argon for the MD simulations, which were performed by the MD package

Key Laboratory for Thermal Science and Power Engineering of Ministry of Education, Department of Engineering Mechanics, Tsinghua University, Beijing 100084, P. R. China. E-mail: caoby@tsinghua.edu.cn; Fax: +86-10-6279-4531; Tel: +86-10-6279-4531

† Electronic supplementary information (ESI) available. See DOI: 10.1039/c5ra18901b

LAMMPS.²⁸ The forces between the argon atoms and between the argon and carbon atoms were calculated based on the Lennard-Jones (LJ) pair potential $\varphi(r) = 4\epsilon \left[\left(\frac{\sigma}{r} \right)^{12} - \left(\frac{\sigma}{r} \right)^6 \right]$. The basic parameters are $\sigma_{\text{Ar-Ar}} = 0.341$ nm, $\epsilon_{\text{Ar-Ar}} = 1.67 \times 10^{-21}$ J, $\sigma_{\text{C-Ar}} = 0.357$ nm, and $\epsilon_{\text{C-Ar}} = 1.97 \times 10^{-21}$ J.^{29,30} The C-C interactions were not considered since the CNT was assumed to be a rigid body,²⁵ so a larger time step of 10 fs could be used in the calculations. The time-consuming calculations of the inter-particle interactions were reduced by using a cutoff distance of 0.77 nm.^{25,29} The NVT canonical ensemble was used with the Nose-Hoover thermostat.

The superimposed simple linear shear flow is illustrated in Fig. 1(b) and in the form of $v_x = \dot{\gamma}y$, $v_y = v_z = 0$, where $\dot{\gamma}$ stands

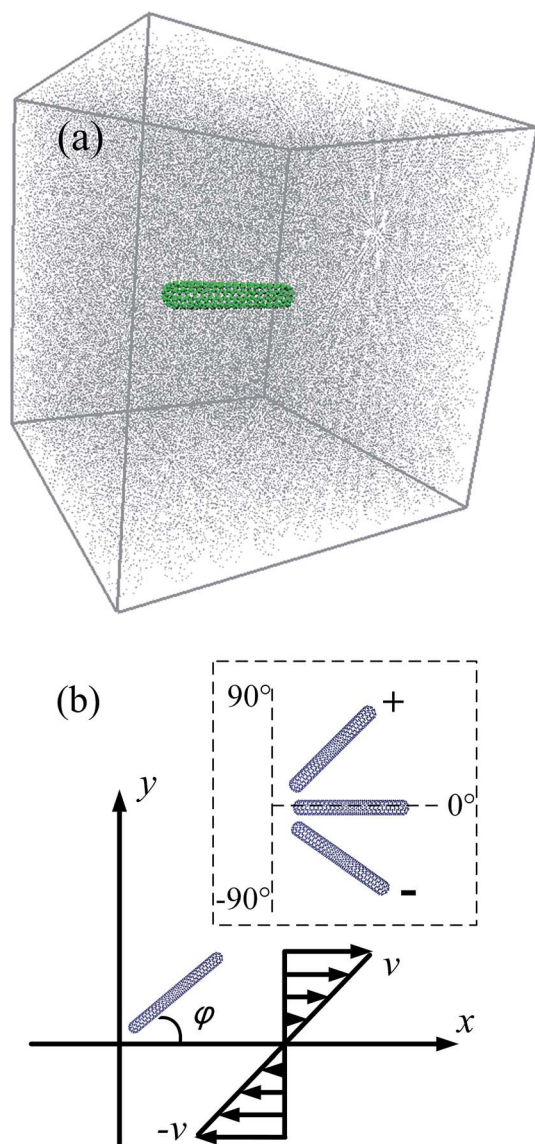


Fig. 1 (a) Schematic diagram of the initial configuration of the MD simulation system; (b) schematic viewing of the applied linear shear in the orthogonal coordinates. The inset inside a dashed rectangle defines the range of CNT's directional angle φ .

for the shear rate. It was realized by utilizing the SLLOD algorithm.³¹ The Lee-Edwards boundary condition³² was applied in the y direction, which is the velocity gradient direction with periodic boundary conditions for the other two directions. The excess heat produced by the shear flow was extracted by the thermostat. The thermostat was only applied in two directions (y, z) and not in the flow direction (x).^{19,33,34} The results were collected after 3×10^5 time steps (3000 ps) to allow time for the flow to develop.

The CNT is confined only to rotate two-dimensionally (2D) on the x - y plane.³⁵ Also shown in Fig. 1(b) is the definition of the CNT's directional angle φ , which is within a range of $(-90^\circ, 90^\circ]$ and $\varphi = 0^\circ$ means the CNT axis is parallel to the flow direction x . To model a rod-shaped object, the CNT was treated as a rigid body. The base case is defined here: the nanotube has the armchair (5, 5) configuration with a diameter, d , of 0.7 nm and length, L , of 4.4 nm. The density, ρ , of the argon is 1091 kg m^{-3} and the temperature, T , is 300 K and the shear rate, $\dot{\gamma}$, is 20.0 GHz. The simulated argon system is in a supercritical state. Later analyses will alter various factors based on the above selected state.

3. Results and discussion

Three types of rotational behavior appear for the time-varying angle, φ , as shown in Fig. 2(a)–(c). The CNT in Fig. 2(a), which has the same state parameters as the base case except for $L = 0.9$ nm, rotates continuously all the time in a clockwise direction, agreeing with the form of the imposed shear in Fig. 1(b). Back-and-force oscillations can be observed in infinitesimal time periods, but the motion is dominated by the unidirectional rotations, one of which is shown in Fig. 2(d). A discontinuous jump exists at -90° to 90° due to the angle definition. While in Fig. 2(b) (the base case), only a few unidirectional rotation periods can be observed and they are interrupted by back-and-force oscillations greatly. No clockwise rotation exists in Fig. 2(c), where the CNT always oscillates around a particular angle when the shear rate $\dot{\gamma} = 50.0$ GHz. The above three rotational types are classified as “continuous rotation”, “interrupted rotation” and “simple oscillation”, respectively, similar to the three orientation types found in our previous three-dimensional rotation study.¹⁹ Considering the potential usage on a CNT-based rotary motor, the continuous rotation state should be paid more attention.

Next, the rotational modes will be decoupled to explore their physical origin as well as to better comprehend and control the above three rotational types. Shown in Fig. 2(b), the labels “1”, “2” and “3” indicate the distinctive segments of the CNT's rotational motion, about to be analyzed one by one in the following discussion. Label “1”: the oscillatory motion between two successive unidirectional rotations. The strength of the oscillation is characterized by the time-averaged frequency f . Label “2”: the total time period T_p of two successive unidirectional rotations and the oscillation in between. The simulation time is prolonged to ensure there are at least 10 individual sets of T_p to achieve its reliable average value. Label “3”: the unidirectional rotation, which is the focus of the present study. We

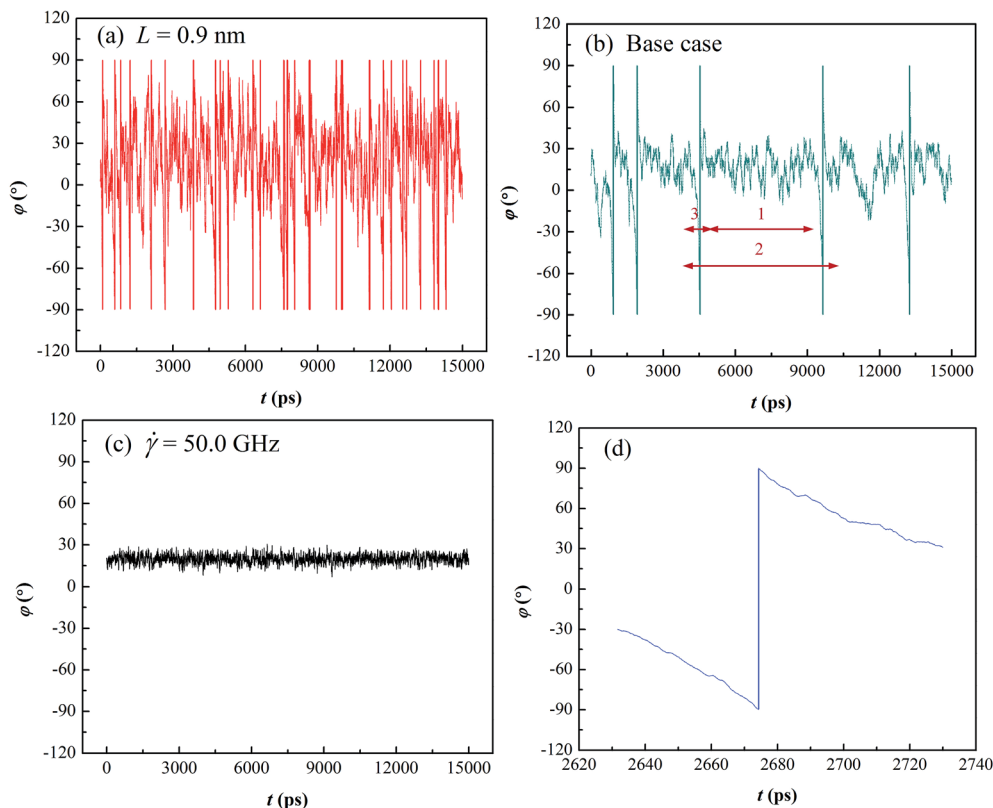


Fig. 2 The time-varying angle φ displays three types of rotational behavior: (a) continuous rotation, (b) interrupted rotation and (c) simple oscillation. The labels “1”, “2” and “3” in (b) respectively indicate the oscillatory motion, two successive unidirectional rotations and the oscillation in between, and the unidirectional rotation. The state parameters are the same as those in the base case, except for (a) CNT length $L = 0.9$ nm, (c) shear rate $\dot{\gamma} = 50$ GHz. (d) is an example of the unidirectional rotation, picked out from (a).

use the angular velocity ω to characterize the unidirectional rotation speed, which was also averaged over 10 individual unidirectional rotations appearing with time. It should be noticed that the boundary between rotation and oscillation is not distinct and there exists a preferred orientation angle around $+10^\circ$ where the CNT oscillates around (Fig. 2(b)). Therefore, the intermediate total rotation angles of 120° , corresponding to the CNT orientation from -30° to 30° (refer to Fig. 2(d)), is used to measure the unidirectional angular velocity ω . As the simple oscillatory state does not exhibit any unidirectional motion (Fig. 2(a)), labels “2” and “3” will not be discussed at that circumstance.

Fig. 3(a) & (b) show the time-averaged oscillatory frequency f (label “1”) versus the rotational diffusion coefficient D_r or shear rate $\dot{\gamma}$. The D_r used is a 2D rotary diffusivity calculated by equilibrium MD method based on the Einstein relation $D_r = \langle (\Delta\varphi)^2 \rangle / 2t$, where $\langle \dots \rangle$ denotes the ensemble average, $\Delta\varphi$ is the angular displacement and t is time.³⁵ Here, we change the CNT length L , diameter d or fluid temperature T of the base case to obtain various D_r values. Interestingly, a positive linear function fits the relationship between the frequency f and D_r very well (Fig. 3(a)), while the frequency does not change with the increase of the shear rate (Fig. 3(b)). The calculated frequency is actually a measure of the strength of the back-and-force oscillation. The monotonic dependence in Fig. 3(a) indicates that in nature the oscillation originates from the rotary Brownian

motion, which can be quantified by the rotational diffusivity D_r . As D_r is a transport coefficient and not affected by the applied shear, the time-averaged frequency will also stay constant when the shear rate changes.

Our current results show that the unidirectional rotations get interrupted occasionally by oscillatory motion, and thus it is not in agreement with the characteristics of continuous Jeffery orbits.²² Note that the CNT approximately experiences 180° during one unidirectional rotation, and then the time elapsed between two successive rotations, *i.e.* T_p (label “2”), may be assumed as the periodic time of the rotating CNT, which can be compared with Jeffery’s theory. For a particle circulating around the Jeffery orbits, $T_p = \frac{2\pi}{\dot{\gamma}} \left(r_e + \frac{1}{r_e} \right)$, where r_e can be expressed as a function of the CNT’s aspect ratio L/d (ref. 23) $r_e = 1.24 \frac{L}{d} \sqrt{\ln \frac{L}{d}}$. The dependence of the periodic time T_p on aspect ratio L/d in Fig. 4(a) exhibits some similar trends, *i.e.* larger L/d leads to larger T_p , as that of the theoretical predictions. However, quantitative agreement is lacking, especially at high shear rate $\dot{\gamma} = 35.0$ GHz. This discrepancy can be further revealed in Fig. 4(b), where T_p first decreases with the increase of the shear rate, in agreement with the theoretical line, while followed by a completely opposite trend at high shear rate. When the shear rate is further increased (>50 GHz), the orientation type of simple oscillation appears and T_p equals to

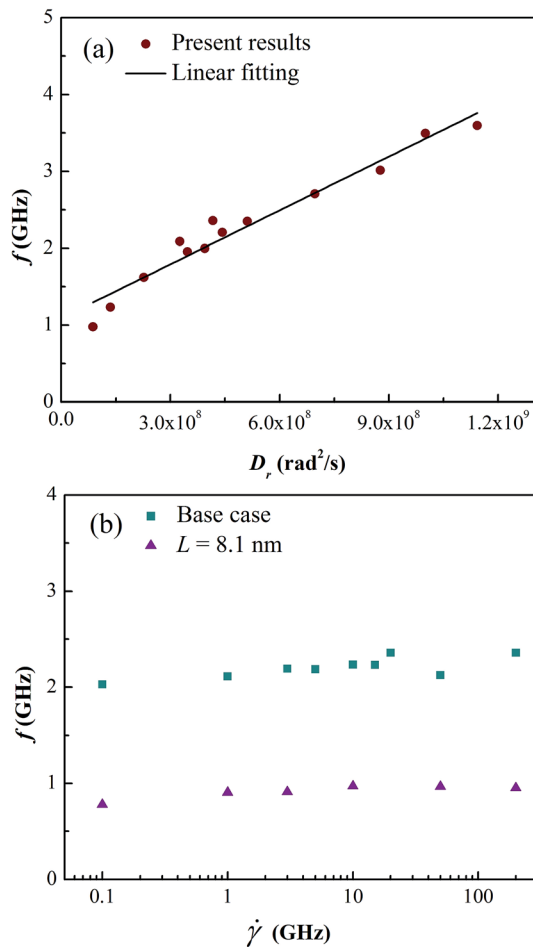


Fig. 3 (a) Dependence of the time-averaged oscillatory frequency f on the rotational diffusion coefficient D_r , along with the linear fitting; (b) dependence of the time-averaged oscillatory frequency f on shear rate $\dot{\gamma}$ for the base case ($L = 4.4$ nm) and the case of $L = 8.1$ nm.

infinity. The above observation thus indicates that the periodic time is not only determined by the applied shear, indicated in Jeffery's theory, but also affected by the rotary Brownian motion, whose presence somehow brings about the unexpected simple oscillatory state and in turn alters the periodic time.

The above calculated periodic time contains the information of both the unidirectional rotations and the oscillatory motion in between. When we focus on the design of a CNT-based motor, the segments of unidirectional rotations are of primary concern. Then, like Fig. 2(d), only the clockwise rotary motion is picked out for analysis (label "3"). Quite different from the dependences of the angular frequency on D_r and $\dot{\gamma}$, the angular velocity ω of the unidirectional rotations does not change with the rotational diffusivity (Fig. 5(a)), *i.e.* ω not affected by the CNT length, diameter and fluid temperature, while it increases linearly with the shear rate (Fig. 5(b)). This evidently suggests that the unidirectional rotation is dominated by the applied shear and not much influenced by the random Brownian motion.

The present shear-induced rotary CNT can yield a clockwise angular velocity as high as 2.86×10^{10} rad s^{-1} at $\dot{\gamma} = 35$ GHz

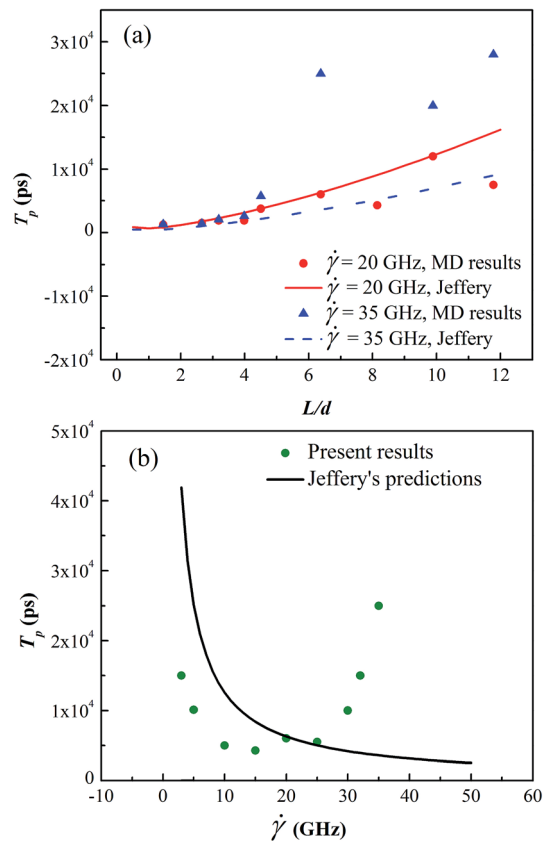


Fig. 4 Dependences of the periodic time T_p (a) on the aspect ratio L/d and (b) on the shear rate $\dot{\gamma}$, compared with Jeffery's predictions.²²

(Fig. 5(b)). When Jeffery's predictions are expressed in terms of the angular velocity, we find that the simulated superhigh angular velocity is larger than those by over one order of magnitude (Fig. 5(b)). As the angular velocity increases with the shear rate, it may be tempting to conclude that the higher shear rate, the faster and more functional rotary motor. This is however not the case because of the occurrence of simple oscillatory state at very high shear ($\dot{\gamma} > 50$ GHz) as previously mentioned. The other limit of very small shear rate ($\dot{\gamma} < 1$ GHz) is not desirable either, for the rotary motion is random and unpredictable, approaching the equilibrium state. Therefore, some intermediate shear rate values should be selected for designing such CNT motor. Moreover, among the three introduced rotational types, the continuous rotating state (Fig. 2(a)) may be preferable, while no clear boundary exists between "interrupted rotation" and "continuous rotation". What we need then is to approach the continuous state, by directly reducing the aspect ratio L/d , reflected by the fact that a smaller L/d brings about a smaller T_p in Fig. 4(a) and thus more circles of clockwise rotations over the same time duration.

Another issue that should be discussed is the very high shear rate used in MD simulations: the shear rates (0.1 – 200 GHz, *i.e.* 1×10^8 to 2×10^{11} s^{-1}) in the present calculations are much higher than those in real cases, *e.g.* experiments on carbon nanotube suspensions, $\dot{\gamma}$: 0.1 s^{-1} to 500 s^{-1} .^{36,37} This high shear was selected to avoid a poor signal to noise ratio, which is

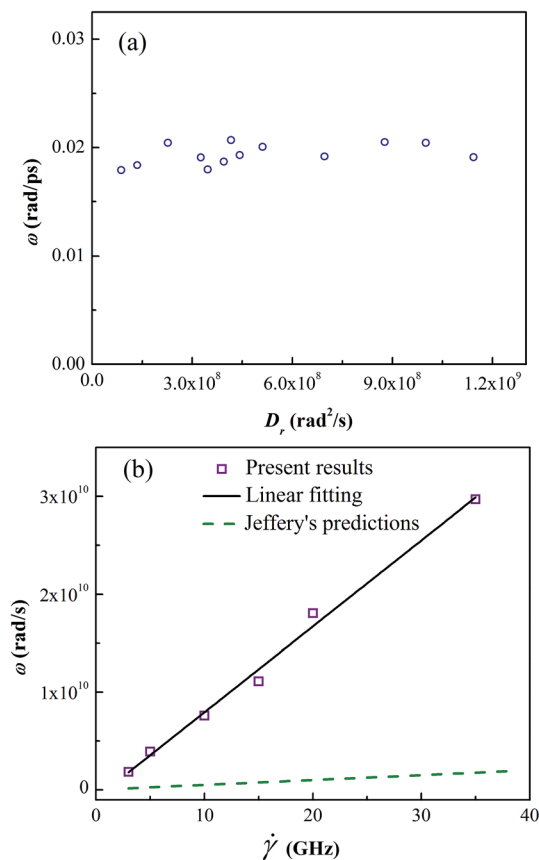


Fig. 5 Dependences of the angular velocity ω of the unidirectional rotation (a) on the rotational diffusion coefficient D_r and (b) on the shear rate $\dot{\gamma}$ along with the linear fitting and Jeffery's predictions.²²

harmful to nonequilibrium MD simulations. If the signal, *i.e.* shear rate, is too small, the established velocity profile will be greatly distorted from the linear shape and the shear-induced results will not be meaningful.³⁸ Moreover, although the GHz value cannot be realized in real experiments, to relate the current study with practical situations we should rather utilize the Peclet number. It is defined as $Pe = \dot{\gamma}/D_r$, and was previously used as a scaling parameter to quantitatively characterize CNT's orientation order under high shear.¹⁹ The above analyses have revealed that the rotational behavior in nature originates from the coupled effects of $\dot{\gamma}$ and D_r , and thus Pe rather than the shear rate should be paid more attention.^{20,39} In our simulations, Pe was in the range of 0–2000. However, in experiments, Pe can be as large as 10^8 (ref. 39) due to a very small D_r . A negative correlation exists between D_r and the particle length. When the length of the particle is at the scale of submicron or micron, D_r can be extremely small and Pe is very large. It is then expected that at similar Pe number, we may find the experimental counterparts of the simulated results.

4. Conclusions

In conclusion, this study analyzes the two-dimensional rotational behavior and dynamics, with special focus on the

unidirectional rotation, of a carbon nanotube in a sheared fluid by molecular dynamics simulations. Three forms of rotational behavior are revealed: “continuous rotation”, “interrupted rotation” and “simple oscillation”. We have decomposed the rotational motion into several features and have distinguished their respective origins: (i) the oscillation stems from rotary Brownian motion; (ii) the angular velocity of the unidirectional rotation is determined by the applied shear; (iii) the periodic time between two successive rotations is affected by both the shear flow and the Brownian rotation. To design a well-constructed CNT nanomotor, two criteria should be achieved: (1) the high rotation speed, *i.e.* angular velocity of the unidirectional motion, which is over one order of magnitude larger than the Jeffery's theory and guaranteed by choosing the shear rate in the range of $3 \text{ GHz} \leq \dot{\gamma} \leq 35 \text{ GHz}$, and can be as high as $\sim 2 \times 10^8 \text{ rad s}^{-1}$; (2) the continuous rotating state, which can be approached by reducing the aspect ratio of CNT. The simulated system may be regarded as the simplest model of a CNT-based rotary motor and the dynamics analyzed here may assist the development of rotational actuators, stirrers, power sources *etc.* used in NEMS, nanofluidics and lab-on-a-chip architectures.

Acknowledgements

This work was supported by the National Natural Science Foundation of China (Grant No. 51322603, 51136001, 51356001), Science Fund for Creative Research Groups (No. 51321002), the Program for New Century Excellent Talents in University, the Tsinghua National Laboratory for Information Science and Technology of China (TNList).

References

- 1 Y. G. Shu, J. C. Yue and Z. C. Ou-Yang, F_0F_1 -ATPase, rotary motor and biosensor, *Nanoscale*, 2010, **2**, 1284–1293.
- 2 H. C. Berg, The rotary motor of bacterial flagella, *Annu. Rev. Biochem.*, 2003, **72**, 19–54.
- 3 E. R. Kay, D. A. Leigh and F. Zerbetto, Synthetic molecular motors and mechanical machines, *Angew. Chem., Int. Ed.*, 2007, **46**, 72–191.
- 4 R. K. Soong, G. D. Bachand, H. P. Neves, A. G. Olkhovets, H. G. Craighead and C. D. Montemagno, Powering an inorganic nanodevice with a biomolecular motor, *Science*, 2000, **290**, 1555–1558.
- 5 R. T. Abraham and R. S. Tibbetts, Cell biology: Guiding ATM to broken DNA, *Science*, 2005, **308**, 510–511.
- 6 J. V. Hernández, E. R. Kay and D. A. Leigh, A reversible synthetic rotary molecular motor, *Science*, 2004, **306**, 1532–1537.
- 7 W. R. Browne and B. L. Feringa, Making molecular machines work, *Nat. Nanotechnol.*, 2006, **1**, 25–35.
- 8 L. Xiao, L. Wei, C. Liu, Y. He and E. S. Yeung, Unsynchronized translational and rotational diffusion of nanocargo on a living cell membrane, *Angew. Chem., Int. Ed.*, 2012, **51**, 4181–4184.

- 9 L. Xiao, Y. Qiao, Y. He and E. S. Yeung, Imaging translational and rotational diffusion of single anisotropic nanoparticles with planar illumination microscopy, *J. Am. Chem. Soc.*, 2011, **133**, 10638–10645.
- 10 K. I. Morozov and A. M. Leshansky, The chiral magnetic nanomotors, *Nanoscale*, 2014, **6**, 1580–1588.
- 11 K. Kim, J. Guo, X. Xu and D. Fan, Micromotors with step-motor characteristics by controlled magnetic interactions among assembled components, *ACS Nano*, 2015, **9**, 548–554.
- 12 J. Guo, K. Kim, K. W. Lei and D. L. Fan, Ultra-durable rotary micromotors assembled from nanoentities by electric fields, *Nanoscale*, 2015, **7**, 11363–11370.
- 13 L. Paterson, M. P. MacDonald, J. Arlt, W. Sibbett, P. E. Bryant and K. Dholakia, Controlled rotation of optically trapped microscopic particles, *Science*, 2011, **292**, 912–914.
- 14 A. M. Popov, Y. E. Lozovik, S. Fiorito and L. Yahia, Biocompatibility and applications of carbon nanotubes in medical nanorobots, *Int. J. Nanomed.*, 2007, **2**, 361–372.
- 15 N. F. Reuel, A. Dupont, O. Thouvenin, D. C. Lamb and M. S. Strano, Three-dimensional tracking of carbon nanotubes within living cells, *ACS Nano*, 2012, **6**, 5420–5428.
- 16 A. Barreiro, R. Rurali, E. R. Hernández, J. Moser, T. Pichler, L. Forró and A. Bachtold, Subnanometer motion of cargoes driven by thermal gradients along carbon nanotubes, *Science*, 2008, **320**, 775–778.
- 17 K. Cai, H. Yin, N. Wei, Z. Chen and J. Shi, A stable high-speed rotational transmission system based on nanotubes, *Appl. Phys. Lett.*, 2015, **106**, 021909.
- 18 S. Pujari, S. S. Rahatekar, J. W. Gilman, K. K. Koziol, A. H. Windle and W. R. Burghardt, Orientation dynamics in multiwalled carbon nanotube dispersions under shear flow, *J. Chem. Phys.*, 2009, **130**, 214903.
- 19 R. Y. Dong and B. Y. Cao, Anomalous orientations of a rigid carbon nanotube in a sheared fluid, *Sci. Rep.*, 2014, **4**, 6120.
- 20 E. K. Hobbie, Shear rheology of carbon nanotube suspensions, *Rheol. Acta*, 2010, **49**, 323–334.
- 21 J. Li, X. Wang, L. Zhao, X. Gao, Y. Zhao and R. Zhou, Rotation motion of designed nano-turbine, *Sci. Rep.*, 2014, **4**, 5846.
- 22 G. B. Jeffery, Motion of ellipsoidal particles immersed in a viscous fluid, *Proc. R. Soc. London, Ser. A*, 1922, **102**, 161–179.
- 23 R. G. Cox, The motion of long slender bodies in a viscous fluid. Part 2. Shear flow, *J. Fluid Mech.*, 1971, **45**, 625–657.
- 24 L. G. Leal and E. J. Hinch, The effect of weak Brownian rotations on particles in shear flow, *J. Fluid Mech.*, 1971, **46**, 685–703.
- 25 W. Tang and S. G. Advani, Nonequilibrium molecular dynamics simulation to describe the rotation of rigid, low aspect ratio carbon nanotubes in simple shear flow, *J. Chem. Phys.*, 2007, **126**, 144711.
- 26 L. B. da Silva, S. B. Fagan and R. Mota, *Ab initio* study of deformed carbon nanotube sensors for carbon monoxide molecules, *Nano Lett.*, 2004, **4**, 65–67.
- 27 G. Shana and S. Bao, The effect of deformations on electronic structures and optical properties of carbon nanotubes, *Physica E*, 2006, **35**, 161–167.
- 28 S. Plimpton, Fast parallel algorithms for short-range molecular dynamics, *J. Comp. Physiol.*, 1995, **117**, 1–19.
- 29 B. Y. Cao and Q. W. Hou, Thermal conductivity of carbon nanotubes embedded in solids, *Chin. Phys. Lett.*, 2008, **25**, 1392–1395.
- 30 R. E. Tuzun, D. W. Noid, B. G. Sumpter and R. C. Merkle, Dynamics of fluid flow inside carbon nanotubes, *Nanotechnology*, 1996, **7**, 241–246.
- 31 D. J. Evans and G. P. Morriss, *Statistical Mechanics of Nonequilibrium Liquids*, Academic, London, 1990.
- 32 A. W. Lee and S. F. Edwards, The computer study of transport processes under extreme conditions, *J. Phys. C: Solid State Phys.*, 1972, **5**, 1921–1929.
- 33 G. S. Grest and K. Kremer, Molecular dynamics simulation for polymers in the presence of a heat bath, *Phys. Rev. A*, 1986, **33**, 3628–3631.
- 34 B. Y. Cao, M. Chen and Z. Y. Guo, Liquid flow in surface-nanostructured channels studied by molecular dynamics simulation, *Phys. Rev. E: Stat., Nonlinear, Soft Matter Phys.*, 2006, **74**, 066311.
- 35 B. Y. Cao and R. Y. Dong, Molecular dynamics calculation of rotational diffusion coefficient of a carbon nanotube in fluid, *J. Chem. Phys.*, 2014, **140**, 034703.
- 36 E. K. Hobbie, H. Wang, H. Kim, S. Lin-Gibson and E. A. Grulke, Orientation of carbon nanotubes in a sheared polymer melt, *Phys. Fluids*, 2003, **15**, 1196–1202.
- 37 M. K. Tiwari, A. V. Bazilevsky, A. L. Yarin and C. M. Megaridis, Elongational and shear rheology of carbon nanotube suspensions, *Rheol. Acta*, 2009, **48**, 597–609.
- 38 B. Y. Cao and R. Y. Dong, Nonequilibrium molecular dynamics simulation of shear viscosity by a uniform momentum source-and-sink scheme, *J. Comp. Physiol.*, 2012, **231**, 5306–5316.
- 39 D. Fry, B. Langhorst, H. Wang, M. L. Becker, B. J. Bauer, E. A. Grulke and E. K. Hobbie, Rheo-optical studies of carbon nanotube suspensions, *J. Chem. Phys.*, 2006, **124**, 054703.